Clay Minerals, (2015) **50**, 199–209

Investigation of the thermal behaviour and decomposition kinetics of kaolinite

XIAOXU LIU, XIAOWEN LIU* AND YUEHUA HU

School of Minerals Processing and Bioengineering, Central South University, Changsha 410083, China

(*Received 16 September 2014; revised 18 April 2015; Editor: G. Christidis*)

ABSTRACT: Previous work on the structural and thermal properties of various types of kaolinite have led to different conclusions, rendering comparison of analytical results difficult. The objectives of the present study were to investigate the thermal behaviour of kaolinite and to carry out a kinetic analysis of the decomposition of kaolinite at high temperatures. X-ray diffraction (XRD), Fourier transform infrared spectroscopy (FTIR) and thermogravimetry-differential scanning calorimetry (TG-DSC) were used to study the mechanism of the thermal decomposition. The modified Coats–Redfern, Friedman, Flynn–Wall–Ozawa and Kissinger decomposition models were used to determine the decomposition mechanism of the kaolinite sample. The dehydroxylation of kaolinite occurred at ~600ºC with the formation of metakaolin, which then transformed into either γ-alumina or aluminium-silicon spinel together with amorphous silica. The results of the XRD and FTIR analyses indicated that the γ-alumina, or aluminium-silicon spinel and amorphous silica phases, transformed into mullite and α-cristobalite, respectively, after decomposition at 900ºC. Good linearity was observed with the modified Coats–Redfern, Flynn–Wall–Ozawa and Kissinger models from room temperature to 1400ºC and the range of the activation energy determined was 120–180 kJ/mol.

KEYWORDS: activation energy, kinetic analysis, thermal decomposition, kaolinite.

Kaolinite, $Al_2Si_2O_5(OH)_4$, is used widely in a variety of industrial applications such as ceramics and refractories, as well as in the paper, rubber, plastics, dyes and paint industries (Murray, 2000; Franco *et al.*, 2004; Scheckel *et al.*, 2010). Its structure has a silicate sheet (Si_2O_5) bonded to a dioctahedral, aluminium hydroxide ($Al_2(OH)_6$, gibbsite) sheet. The thermal treatment of kaolinite shows considerable complexity with regard to the non-stoichiometric composition of the products, the pre-dehydroxylation process (Shvarzman *et al.*, 2003), the gradual disappearance of residual hydroxyl groups (Balek & Murat, 1996) and the formation of mullite (Chakraborty, 2003). The process is also influenced by the intrinsic properties of the kaolinite, such as the degree of disorder within the kaolinite structure (Heide & Földvari, 2006), by pressure and partial water vapour pressure (Nahdi *et al.*, 2002; Reynolds & Bish, 2002), by heating rate (Castelein *et al.*, 2001), mechanical treatments (Amina *et al.*, 2014) and ultrasound processing (Pérez-Rodríguez *et al.*, 2006) of the sample. Therefore, the possible changes in the properties of kaolinite during high-temperature calcination have received considerable attention.

The thermal reactions of kaolinite can be divided into four steps, namely a low-temperature reaction at <400ºC, intermediate-temperature reactions, mainly between 400–650ºC, high-temperature reactions at >700ºC and oxidation reactions (Brindley & Nakahira 1957). Wang *et al.* (2011) focused on the thermal behaviour of kaolin and the decomposition

* E-mail: lxwdr@csu.edu.ca
DOI: 10.1180/claymin.2015.050.2.04

behaviour of kaolin by simultaneous thermogravimetry-differential thermal analysis (TG-DTA) experiments. Cheng *et al.* (2012) reviewed the thermal behaviour of kaolinite complexes intercalated with the most common reagents and summarized their thermal behaviour. The phase transformations were influenced by the degree of disorder in the kaolinite structure, the formation environment and the amount and the type of impurities. The kinetics of the dehydroxylation have also been studied extensively; due to the aforementioned factors, however, it has been difficult to propose a single value of the overall activation energy. The published values of the activation energy range from 120 to 250 kJ/mol (Prodanović *et al.*, 1989; Levy & Hurst, 1993; Nahdi *et al.*, 2002; Traoré *et al.*, 2006; Ptáček *et al.*, 2010b, 2011).

The objectives of the present study were to obtain insights into the thermal behaviour of kaolinite, to carry out kinetic analysis of its decomposition at high temperatures and to test the applicability of the modified Coats–Redfern, Friedman, Flynn–Wall–Ozawa and Kissinger decomposition models to kaolinite.

EXPERIMENTAL

Materials and methods

The material used was a kaolin from Maoming, Guangdong, China containing ~96% kaolinite with minor quartz. The chemical composition listed in Table 1 confirms that the material is composed essentially of kaolinite; therefore, the term kaolinite will be used instead of kaolin. After drying at 60ºC, the kaolinite was ground with a planetary ball mill to pass through a 0.074 mm sieve. All subsequent experiments were performed using this ground kaolinite sample.

The original kaolinite samples (4 g) were heated in a programmable, temperature-controlled muffle furnace for 2.5 h, at a heating rate of 10ºC/min from 200–1400ºC. The fired products were ground into powders using an agate mortar and were labelled with the heating temperature in ºC.

The 1400ºC sample (2 g) was digested with 85% orthophosphoric acid (H_3PO_4) (100 mL) by heating rapidly to 240ºC for 12 min. The viscous suspension was cooled to 60ºC, diluted to 800 mL with distilled water and filtered. The residue was washed with distilled water to remove the excess PO_4^{3-} ions and dried at room temperature to give the sample labelled K0.

Characterization techniques

X-ray diffraction (XRD) patterns were obtained with a DX-2700 diffractometer (Dandong Haoyuan Instrument Co. Ltd., China) at 40 kV, 40 mA and a scanning rate of 9º/min, using Ni-filtered CuKα radiation (λ = 1.5418 Å). Fourier-transform infrared (FTIR) spectra were recorded using KBr pellets (0.9 mg sample with 80 mg KBr) on a Nicolet 5700 spectrophotometer (Thermo Nicolet, USA). The TG-DSC was performed using a Netzch STA449C thermal analyser (Netzsch, Germany) at a heating rate of 12ºC/min under a N_2 flow (20 cm^3/min), using 10 mg samples and α-Al_2O_3 as inert pan material. The chemical composition of the samples was determined using X-ray fluorescence (XRF), on an Axios^{mAX} instrument (PANalytical, The Netherlands).

Theoretical approaches

The fundamental rate equation used for all kinetic studies was (Šesták, 1984; Yao *et al.*, 2008; Liu *et al.*, 2010):

$$d\alpha/dt = kf(\alpha) \quad (1)$$

where k is the rate constant, which is a function of reaction temperature and f(α) is the reaction model, a function dependent on the actual reaction mechanism. Equation 1 expresses the rate of conversion, dα/d*t*, at a constant temperature as a

TABLE 1. Chemical composition of the original kaolinite sample by XRF (mass%).

Sample	SiO_2	MgO	Al_2O_3	Fe_2O_3	Na_2O	CaO	TiO_2	K_2O	LOI
kaolinite	46.38	0.14	38.40	0.69	0.19	0.01	0.29	0.38	13.26

https://doi.org/10.1180/claymin.2015.050.2.04 Published online by Cambridge University Press

function of the reactant concentration loss and rate constant. In this study, the conversion rate α is defined as:

$$\alpha = (W_0 - W_t)/(W_0 - W_f) \quad (2)$$

where W_t, W_0 and W_f are the weight at time t and the initial and final weights of the sample, respectively. The rate constant k is given by the Arrhenius equation:

$$k = A \exp(-E/RT) \quad (3)$$

where E is the apparent activation energy (kJ/mol), R is the gas constant (8.314 J/K mol), A is the pre-exponential factor (min^{-1}) and T is the absolute temperature (K). The combination of equations 1 and 3 yields:

$$d\alpha/dt = A \exp(-E/RT) f(\alpha) \quad (4)$$

For a constant heating rate $\beta = dT/dt$. Introducing β into equation 4 yields equation 5:

$$d\alpha/dT = (A/\beta) \exp(-E/RT) f(\alpha) \quad (5)$$

Equations 4 and 5 are the fundamental expressions used to calculate the kinetic parameters based on DSC data. Various models have been developed based on these fundamental equations and the most common model methods were also used in this study (Table 2). The Friedman method (Friedman, 1964) is an iso-conversional method, which yields $(-E/R)$ directly for a given value of α by plotting $\ln(d\alpha/dt)$ *vs.* $1/T$. The modified Coats–Redfern method (Brown *et al.*, 2000) is a multi-heating rate application of the Coats–Redfern equation. Plotting the left side of the equation for each heating rate *vs.* $1/T$ at that heating rate provides a group of straight lines of slope $-E/R$. The full solution has to be done iteratively by first assuming a value of E and then recalculating the left side of the equation until convergence occurs. However, a quick solution is also available by moving $(1-2RT/E)$ into the intercept and assuming that it is a constant. The iso-conversional Flynn–Wall–Ozawa method (Ozawa, 1965; Flynn & Wall, 1966) is an integral method, which yields $-E/R$ from the slope of the line determined by plotting logβ against $1/T$ at a given conversion rate. In the Kissinger method (1956), $\ln(\beta/T_m^2)$ is plotted against $1/T_m$ for a series of experiments at different heating rates, with the peak temperature, T_m, obtained from the DSC curve.

RESULTS AND DISCUSSION

XRD results

The XRD pattern of the original kaolin (Fig. 1a) confirms the predominance of kaolinite (JCPDS 80-0886) in the sample. Heating from 200–500ºC, did not affect the positions of the kaolinite peaks significantly. The decrease in the intensity and broadening of the diffraction lines after calcination, especially the (001) reflection at 12.4º2θ, is attributed to a decrease in crystal order (Yang *et al.*, 2006). This change in "crystallinity" has been used to quantify the progressive structural damage (Aglietti & Lopez, 1992). The "crystallinity" index is defined as: $C = B_0I/(I_0B) \times 100\%$, where C is the 'crystallinity' (degree of crystal order), B_0 is the background intensity of the original sample, I is the peak intensity of the thermally treated material, I_0 is the peak intensity of the original material and B is the background intensity of the thermally treated material. The degree of crystal order compared to the (001) diffraction maximum of the original kaolinite and the samples heated at 200ºC, 300ºC, 400ºC and 500ºC were 100, 84.7, 76.0, 57.8 and 56.0%, respectively. Moreover, with increasing heating temperature from 200–500ºC, the d spacings of the diffraction maxima decreased (Table 3). For example, the d_{001} decreased from 0.716 to 0.709 nm, the $d_{\bar{1}10}$ from 0.436 to 0.433 nm

TABLE 2. Kinetic models used to evaluate the activation energy, E.

Methods	Expression	Plots
Friedman	$\ln(d\alpha/dt) = \ln(Af(\alpha)) - E/RT$	$\ln(d\alpha/dt)$ *vs.* $1/T$
Coats–Redfern (modified)	$\ln[\beta/T^2(1 - 2RT/E)] = \ln[- AR/E\ln(1 - \alpha)] - E/RT$	$\ln[\beta/T^2]$ *vs.* $1/T$
Flynn–Wall–Ozawa	$\log\beta = \log[AE/Rg(\alpha)]^* - 0.4567E/RT - 2.315$	$\log\beta$ *vs.* $1/T$
Kissinger	$\ln(\beta/Tm^2) = -E/RT_m + \ln(AR/E)$	$\ln(\beta/T_m^2)$ *vs.* $1/T$

* where $g(\alpha)$ is the integral form of $f(\alpha)$.

https://doi.org/10.1180/claymin.2015.050.2.04 Published online by Cambridge University Press

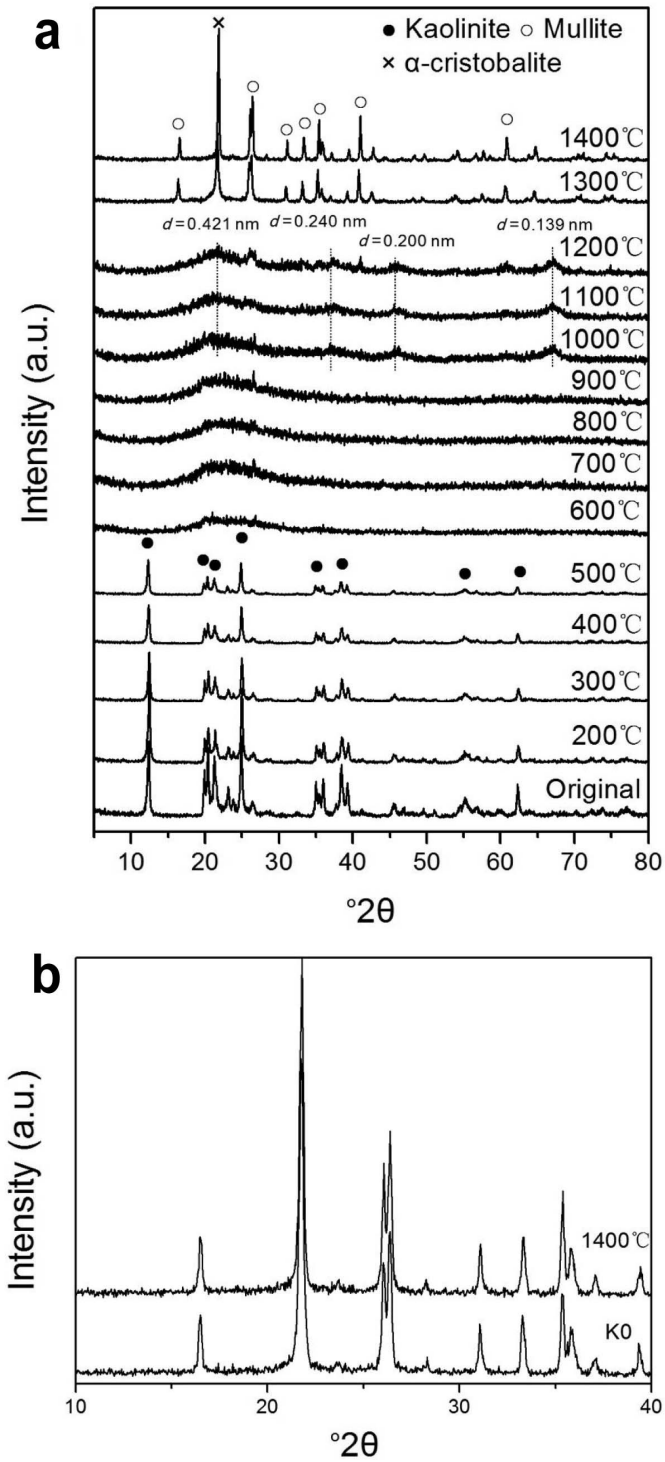

FIG. 1. XRD patterns of (a) the original kaolinite heated at different temperatures and (b) of the H_3PO_4-treated sample as prepared (K0) and after heating at 1400ºC.

https://doi.org/10.1180/claymin.2015.050.2.04 Published online by Cambridge University Press

TABLE 3. Evolution of the *d* spacings of the kaolinite heated at different temperatures.

Samples	d_{001} (nm)	$d_{\bar{1}10}$ (nm)	d_{002} (nm)
Original kaolinite	0.716	0.436	0.357
200ºC	0.715	0.436	0.357
300ºC	0.714	0.435	0.356
400ºC	0.711	0.434	0.356
500ºC	0.709	0.433	0.356

and the d_{002} from 0.357 to 0.356 nm. Dehydration of the kaolinite occurred at 200–500ºC.

When calcined at 600ºC, the diffraction maxima ascribed to the kaolinite disappeared due to a transformation of kaolinite into metakaolinite (Wang *et al.*, 2011). The XRD pattern of the sample heated at 1000ºC showed a broad reflection centred at 21.1º2θ (d = 0.421 nm), which was attributed to amorphous metakaolinite. The reflections corresponding to d spacings of 0.240, 0.200 and 0.139 nm (37.5, 45.5 and 67.1º2θ, respectively), were assigned to γ-Al_2O_3 (JCPDS 10-0425) or aluminium-silicon spinel (Brindley, 1976). An additional weak peak observed at 26.2º2θ in the 1200ºC sample, was due to mullite (JCPDS 83-1881), the intensity of which increased with increasing temperature. Another new weak peak at 21.7º2θ in the 1300ºC and 1400ºC samples, was assigned to α-cristobalite (JCPDS 39-1425) formed after calcination at 1300ºC. Due to the similarity of their XRD patterns, well ordered opal-C and opal-CT may be misidentified as α-cristobalite (Önal *et al.*, 2007a). Phosphoric acid digestion may assist detection of the α-cristobalite phase, thus the K0 sample yielded an XRD pattern with the characteristic d_{101} peak of α-cristobalite, 0.408 nm. After H_3PO_4-digestion, the position, intensity and half-width at maximum peak height (FWHM) of the (101) reflection did not change (Fig. 1b), suggesting the presence of α-cristobalite (Sarikaya *et al.*, 2000; Önal & Sarikaya, 2007b).

FTIR analysis

Heating at different calcination temperatures altered the FTIR spectra of the kaolinite samples (Fig. 2). The original kaolinite displayed characteristic bands at 428 (Si–O), 539 (Al–O–Si) and 698 cm^{-1} (Al–O) (Madejová, 2003; Hu & Yang, 2010). The band at 914 cm^{-1} is attributed to the bending vibration of the inner Al–OH groups of the octahedral layer. As the temperature increased from 200–500ºC, the intensity of the Al–O–Si deformation vibration at 539 cm^{-1} decreased, indicating that dehydroxylation was accompanied by destruction of Al–O–Si linkages of the kaolinite. Compared to the 500ºC sample, the IR spectrum of the 600ºC sample displayed two weaker bands at 467 and 3619 cm^{-1}, which originated from the Si–O–Si stretching vibration and the inner Al–OH stretching vibration, respectively (Dellisanti *et al.*, 2009; Ríos *et al.*, 2009). The decreasing intensity of these two bands can be attributed to dehydroxylation of the kaolinite

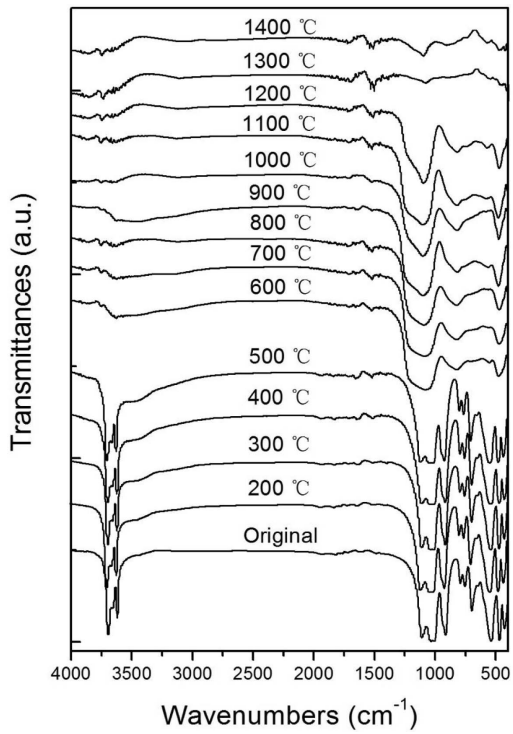

FIG. 2. FTIR spectra of the kaolinite samples heated at different temperatures

https://doi.org/10.1180/claymin.2015.050.2.04 Published online by Cambridge University Press

at 600ºC. Furthermore, the two new bands at 813 and 1071 cm^{-1}, are assigned to the typical Si−O−Al and Si−O−Si stretching vibrations of metakaolin. The vibration band at 914 cm^{-1} disappeared because of the removal of hydroxyl groups (Kakali *et al.*, 2001). The intensity of the Si−O−Si asymmetric stretching vibration at 1071 cm^{-1} increased over the range 600−900ºC and the location shifted from 1071−1092 cm^{-1} due to the progressive disordering of the kaolinite with increasing temperature. The band at 560 cm^{-1}, which appeared in the spectrum of the 900ºC sample was assigned to Al−O stretching associated with octahedrally coordinated Al^{VI} in γ-Al_2O_3 (Voll *et al.*, 2001). Therefore, this band reflected the formation of nano-crystalline γ-Al_2O_3. A well resolved peak at 571 cm^{-1}, observed in the spectra of samples heated at 1300 and 1400ºC, is typical of Al^{VI}−O stretching in mullite (Voll *et al.*, 2002). A Si−O−Si bending band at 471 cm^{-1}, broadened with increasing temperature from 500−800ºC and shifted gradually from 471 to 462 cm^{-1}, reflecting the progressive disordering of metakaolin and the increase of the mean bond angle in the Si−O−Si network. In the sample heated at 1200ºC, the intensity of the Si−O−Si stretching band at 469 cm^{-1} increased due to formation of amorphous silica (Zhuravlev, 1993). The transformation of amorphous silica to α-cristobalite occurred between 1200 and 1300ºC as was suggested by the appearance of the band at 794 cm^{-1}, attributed to α-cristobalite (Mollah *et al.*, 1999).

DSC analysis

The TG-DSC curves of the original kaolinite (Fig. 3) showed a broad endothermic peak at

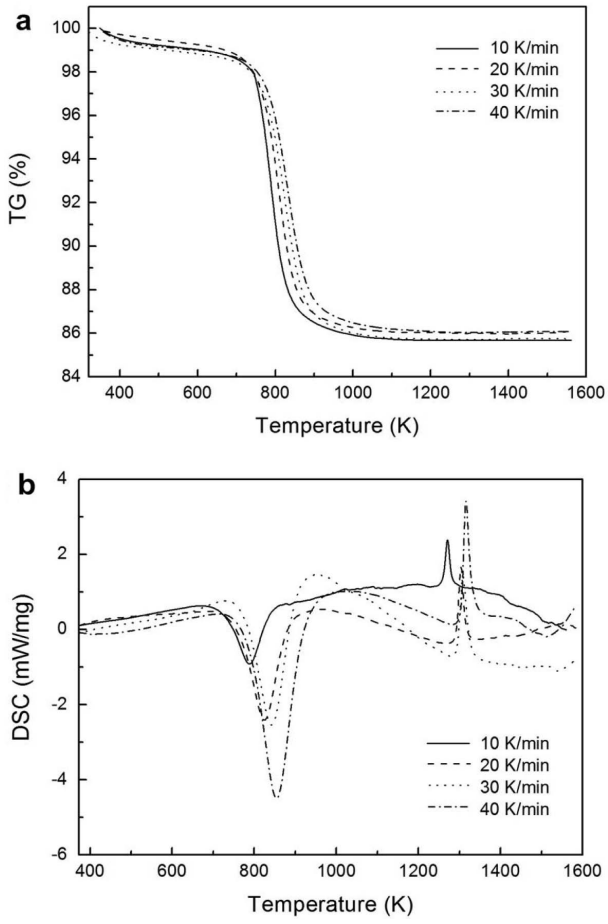

FIG. 3. (a) TG and (b) DSC curves of the kaolinite sample at different heating rates

https://doi.org/10.1180/claymin.2015.050.2.04 Published online by Cambridge University Press

500–600ºC due to the dehydroxylation of the kaolinite (equation 6). The corresponding dehydroxylation peak temperatures (T_m) were 515, 541, 561 and 570ºC, at heating rates of 10, 20, 30 and 40 K/min, respectively. The exothermic peaks above 1000ºC were ascribed to the formation of mullite and amorphous silica (Badogiannis *et al.*, 2005). α-cristobalite was formed from the amorphous silica phase at 1300ºC. The following reactions took place at high temperatures (Balek *et al.*, 1996; Chakraborty, 2003):

$$Al_2Si_2O_5(OH)_4 \rightarrow Al_2Si_2O_7 \text{ (metakaolin)} + 2\ H_2O\ (g) \quad (6)$$

$$Al_2Si_2O_7 \text{ (metakaolin)} \rightarrow SiAl_2O_5 \text{ (spinel)} + SiO_2 \text{ (amorphous)} \quad (7a)$$

or

$$Al_2Si_2O_7 \text{ (metakaolin)} \rightarrow Al_2O_3 \text{ (γ-alumina)} + 2\ SiO_2 \text{ (amorphous)} \quad (7b)$$

$$3\ SiAl_2O_5 \text{ (spinel)} \rightarrow Al_6S_2iO_{13} \text{ (mullite)} + SiO_2 \text{ (amorphous)} \quad (8a)$$

or

$$3\ Al_2O_3 \text{ (γ-alumina)} + 2\ SiO_2 \text{ (amorphous)} \rightarrow Al_6S_2iO_{13} \text{ (mullite)} \quad (8b)$$

$$SiO_2 \text{ (amorphous)} \rightarrow SiO_2 \text{ (α-cristobalite)} \quad (9)$$

The approximate temperatures at which the reactions outlined in equations 6–9 occurred, were 600, 900, 1100 and 1300ºC, respectively, and were in accord with Jasmund & Lagaly, (1993), who reported decomposition of kaolinite and formation of metakaolin at 450ºC. The transformation of the metakaolinite to spinel occurs at 900–1200ºC.

Kinetics of the decomposition reaction of kaolinite

Kinetic studies use either differential or integral approaches (Tang *et al.*, 2003). In the present investigation the integral approaches, the Coats–Redfern, Friedman and Flynn–Wall–Ozawa methods, were applied to investigate the decomposition kinetics of kaolinite. The decomposition of kaolinite is a typical example of a solid-state reaction that follows first-order kinetics (Brindley *et al.*, 1957). In order to confirm the mechanism, the relationship between the kaolinite transformation rate (α) and the reaction temperature (T) was used (Table 4).

The iso-conversional plots based on the modified Coats–Redfern, Friedman and Flynn–Wall–Ozawa methods showed an overall trend in activation energy (Fig. 4) for the kaolinite. Approximately linear relationships were observed for conversion rates, α, of 0.1–0.6, corresponding to temperatures of 487–591ºC. The lines fitted were nearly parallel, which indicated that the activation energies varied almost linearly with conversion rates and consequently implied the possibility of a single reaction mechanism (or the unification of multiple-reaction mechanisms) (Yao *et al.*, 2008; Liu *et al.*, 2010). However, a different reaction mechanism may be occurring at conversion rates outside the range $0.1 < \alpha > 0.6$, due to the obviously non-parallel lines. The change in the reaction mechanism at low and high conversion rates might be due to the particle size distribution (Johnson & Kessler, 1969) or to a change in the mechanism occurring at high conversion factors (Criado *et al.*, 1984). The curves derived from the modified Coats–Redfern and the Flynn–Wall–Ozawa methods showed more clearly parallel trends than those from the Friedman

TABLE 4. The relationship between the kaolinite samples' transformation rate (α) and reaction temperature (T) at different heating rates.

						T/K					
β	α =	α =	α =	α =	α =	α =	α =	α =	α =	α =	α =
(K min^{-1})	0%	10%	20%	30%	40%	50%	60%	70%	80%	90%	100%
10	725	748	760	771	779	786	794	802	811	825	853
20	747	768	782	792	800	808	816	824	834	849	881
30	766	785	798	808	817	825	834	843	854	869	900
40	773	788	805	816	825	833	843	853	864	881	918

https://doi.org/10.1180/claymin.2015.050.2.04 Published online by Cambridge University Press

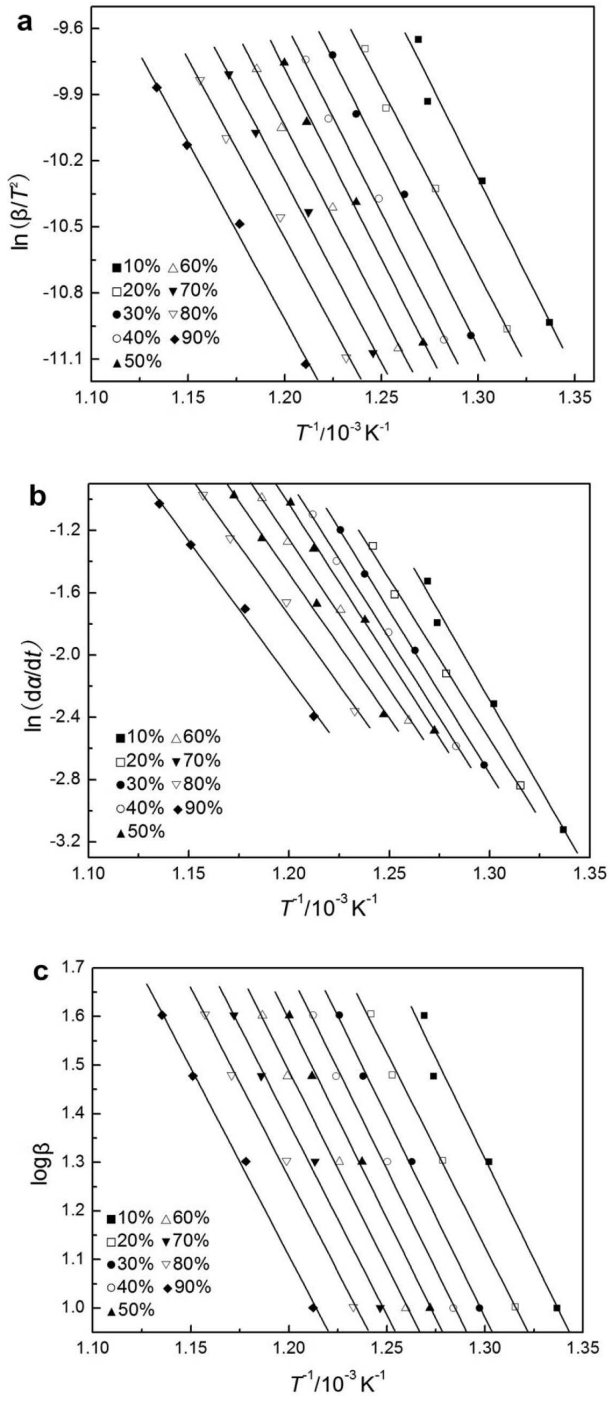

FIG. 4. Plot of the activation energies (E) of the kaolinite sample for different conversion rates by (a) the modified Coats–Redfern, (b) the Friedman and (c) the Flynn–Wall–Ozawa methods

https://doi.org/10.1180/claymin.2015.050.2.04 Published online by Cambridge University Press

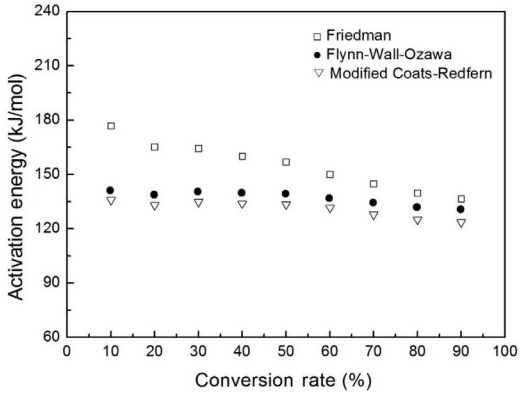

FIG. 5. A comparison of apparent activation energy (E) as a function of decomposition conversion rate (a) for kaolinite calculated by (a) the modified Coats–Red-Redfern, (b) the Friedman and (c) the Flynn–Wall–Ozawa methods

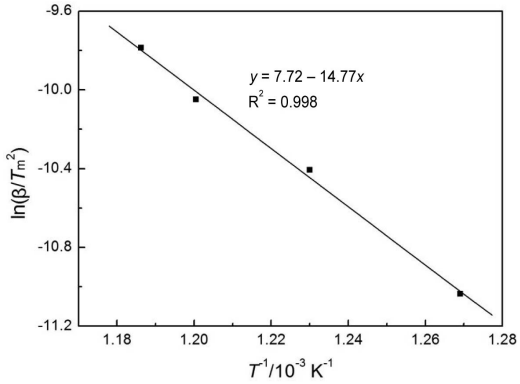

FIG. 6. Plot of the activation energy of the kaolinite sample calculated by the Kissinger method

method (Fig. 4). The average E of all conversion rates calculated with the modified Coats–Redfern method, 134.0 kJ/mol and with the Flynn–Wall–Ozawa method was 139.6 kJ/mol. The E values obtained, based on these two methods, were in the range 120–150 kJ/mol, both lower than the results from the Friedman method (Fig. 5).

The linear plot of $\ln[\beta/T_m^2]$ *vs.* $1/T_m$, based on the Kissinger method, is shown in Fig. 6. The Kissinger method is not a model-free method, but can be used for determining the value of E and the overall trend of E *vs.* T when specific conversion rate factors are used (Yao *et al.*, 2008) and the value of E is stable over the conversion range. From the DSC curves of the kaolinite samples at different heating rates, the best linearity of $\ln[\beta/T_m^2]$ *vs.* $1/T_m$ might be chosen and the activation energy might be calculated. The E value was calculated as 122.8 kJ/mol, which is in agreement with the other models.

The modified Coats–Redfern and Flynn–Wall–Ozawa methods showed better parallel trends than the Friedman method (Fig. 4) and both gave constant values of E (Fig. 5). To confirm a possible mechanism, the different kinetic analysis methods should be complementary rather than competitive (Brown *et al.*, 2000). Therefore, an appropriate apparent activation energy range should be obtained by combining all observations (Figs 4 and 6) and, consequently, a general activation energy range of 120–180 kJ/mol is suggested for the kaolinite decomposition reaction. This general range might offer a somewhat narrower range of activation energy for understanding kaolinite decomposition with respect to values reported previously, e.g. 20–250 kJ/mol (Ptáček *et al.*, 2010a). The activation energy of a reaction might provide the critical information of the minimum energy necessary for starting a particular reaction and the energy range for decomposition obtained in this study may assist in understanding the thermal stability of the kaolinite.

CONCLUSIONS

TG-DSC was used to investigate the thermal decomposition of kaolinite at different heating rates under a nitrogen atmosphere and data from XRD and FTIR analyses were used to confirm the decomposition. Kaolinite was transformed to metakaolin on heating to 600ºC and the peak temperature of the dehydroxylation was at ~500ºC. The metakaolin transformed into γ-alumina, or aluminium-silicon spinel and amorphous silica after decomposition at 900ºC. The reaction kinetics model of kaolinite decomposition in a solid-state reaction was investigated based on the modified Coats–Redfern, Friedman, Flynn–Wall–Ozawa and Kissinger models. The first-order mechanism of the decomposition of the kaolinite was confirmed and the activation energy was estimated to be 120–180 kJ/mol.

ACKNOWLEDGMENTS

This work was supported by the National Twelfth Five-year Science and Technology Support Program

https://doi.org/10.1180/claymin.2015.050.2.04 Published online by Cambridge University Press

(2012BAB10B00) and the China Scholarship Council (CSC).

REFERENCES

Aglietti E.F. & Lopez J.P. (1992) Physicochemical and thermal properties of mechanochemically activated talc. *Materials Research Bulletin*, **27**, 1205–1216.

Amina B., Sahnoun R.D. & Bouaziz J. (2014) Effects of mechanochemical treatment on the properties of kaolin and phosphate-kaolin materials. *Powder Technology*, **264**, 477–483.

Badogiannis E., Kakali G. & Tsivilis S. (2005) Metakaolin as supplementary cementitious material – Optimization of kaolin to metakaolin conversion. *Journal of Thermal Analysis and Calorimetry*, **81**, 457–462.

Balek V. & Murat M. (1996) The emanation thermal analysis of kaolinite clay minerals. *Thermochimica Acta*, **282–283**, 385–397.

Brindley G.W. (1976). Thermal transformations of clays and layer silicates. Pp. 119–130 in: *Proceedings of the International Clay Conference*, (S.W. Bailey editor). Mexico City, Mexico, 1965, Applied Publishing, Wilmette, Illinois, USA.

Brindley G.W. & Nakahira M. (1957) Kinetics of dehydroxylation of kaolinite and halloysite. *Journal of the American Ceramic Society*, **40**, 346–350.

Brown M.E., Maciejewski M., Vyazovkin S., Nomen R., Sempere J., Burnham A., Opfermann J., Strey R. Anderson H L., Kemmler A., Keuleers R., Janssens J., Desseyn H.O., Li C.-R., Tang T.B., Roduit B., Malek J. & Mitsuhashi T. (2000) Computational aspects of kinetic analysis. Part A: The ICTAC kinetics project-data, methods and results. *Thermochimica Acta*, **355**, 125–143.

Castelein O., Soulestin B., Bonnet J.P. & Blanchart P. (2001) The influence of heating rate on the thermal behaviour and mullite formation from a kaolin raw material. *Ceramics International*, **27**, 517–522.

Chakraborty A.K. (2003) DTA study of preheated kaolinite in the mullite formation region. *Thermochimica Acta*, **398**, 203–209.

Cheng H.F., Liu Q.F., Yang J., Ma S.J. & Frost R.L. (2012) The thermal behavior of kaolinite intercalation complexes – A review. *Thermochimica Acta*, **545**, 1–13.

Criado J.M., Ortega A., Real C. & Torres de Torres E. (1984) Reexamination of the kinetics of the thermal dehydroxylation of kaolinite. *Clay Minerals*, **19**, 653–661.

Dellisanti F., Valdrè G. & Mondonico M. (2009) Changes of the main physical and technological properties of talc due to mechanical strain. *Applied Clay Science*, **42**, 398–404.

Flynn J.H. & Wall L.A. (1966) General treatment of thermogravimetry of polymers. *Journal of Research of the National Bureau of Standards Section A: Physical Chemistry*, **A70**, 487–523.

Franco F., Pérez-Maqueda L.A. & Pérez-Rodríguez J.L. (2004) The effect of ultrasound on the particle size and structural disorder of a well-ordered kaolinite. *Journal of Colloid and Interface Science*, **274**, 107–117.

Friedman H.L. (1964) Kinetics of thermal degradation of char-forming plastics from thermogravimetry. Application to a phenolic plastic. *Journal of Polymer Science Part C: Polymer Symposia*, **6**, 183–195.

Heide K. & Földvari M. (2006) High temperature mass spectrometric gas-release studies of kaolinite $Al_2[Si_2O_5(OH)_4]$ decomposition. *Thermochimica Acta*, **446**, 106–112.

Hu P.W. & Yang H.M. (2010) Controlled coating of antimony-doped tin oxide nanoparticles on kaolinite particles. *Applied Clay Science*, **48**, 368–374.

Jasmund K. & Lagaly G. (1993) *Tonminerale und Tone*. Steinkopf Verlag. Darmstadt, Germany.

Johnson H.B. & Kessler F. (1969) Kaolinite dehydroxylation kinetics. *Journal of the American Ceramic Society*, **52**, 199–203.

Kakali G., Perraki T., Tsivilis S. & Badogiannis E. (2001) Thermal treatment of kaolin: the effect of mineralogy on the pozzolanic activity. *Applied Clay Science*, **20**, 73–80.

Kissinger H.E. (1956) Variation of peak temperature with heating rate in differential thermal analysis. *Journal of Research of the National Bureau of Standards*, **57**, 217–221.

Levy J.H. & Hurst H.J. (1993) Kinetics of dehydroxylation, in nitrogen and water vapour, of kaolinite and smectite from Australian Tertiary oil shales. *Fuel*, **72**, 873–877.

Liu X.X., Yu L., Xie F.W., Li M., Chen L. & Li X.X. (2010) Kinetics and mechanism of thermal decomposition of cornstarches with different amylose/amylopectin ratios. *Starch-Starke*, **62**, 139–146.

Madejová J. (2003) FTIR techniques in clay mineral studies. *Vibrational Spectroscopy*, **31**, 1–10.

Mollah M.Y.A., Promreuk S., Schennach R., Cocke D.L. & Güler R. (1999) Cristobalite formation from thermal treatment of Texas lignite fly ash. *Fuel*, **78**, 1277–1282.

Murray H.H. (2000) Traditional and new applications for kaolin, smectite and palygorskite: a general overview. *Applied Clay Science*, **17**, 207–221.

Nahdi K., Llewellyn P., Rouquérol F., Rouquérol J., Ariguib N.K. & Ayedi M.T. (2002) Controlled rate thermal analysis of kaolinite dehydroxylation: effect of water vapour pressure on the mechanism. *Thermochimica Acta*, **390**, 123–132.

Önal M., Kahraman S. & Sarıkaya Y. (2007a) Differentiation of α-cristobalite from opals in

bentonites from Turkey. *Applied Clay Science*, **35**, 25–30.

Önal M. & Sarikaya Y. (2007b) The effect of heat treatment on the paracrystallinity of an opal-CT found in a bentonite. *Journal of Non-Crystalline Solids*, **353**, 4195–4198.

Ozawa T. (1965) A new method of analyzing thermogravimetric data. *Bulletin of the Chemical Society of Japan*, **38**, 1881–1886.

Pérez-Rodríguez J.L., Pascual J., Franco F., Jiménez de Haro M.C., Duran A., Ramírez del Valle V. & Pérez-Maqueda L.A. (2006) The influence of ultrasound on the thermal behaviour of clay minerals. *Journal of the European Ceramic Society*, **26**, 747–753.

Prodanović D., Živković Ž.D. & Dumić M. (1989) The kinetics of dehydroxylation and mullitization of zettlitz kaolin in the presence of calcium(II) as an ingredient. *Thermochimica Acta*, **156**, 61–67.

Ptáček P., Kubátová D., Havlica J., Brandštetr J., Šoukal F. & Opravil T. (2010a) Isothermal kinetic analysis of the thermal decomposition of kaolinite: the thermogravimetric study. *Thermochimica Acta*, **501**, 24–29.

Ptáček P., Kubátová D., Havlica J., Brandštetr J., Šoukal F. & Opravil T. (2010b) The non-isothermal kinetic analysis of the thermal decomposition of kaolinite by thermogravimetric analysis. *Powder Technology*, **204**, 222–227.

Ptáček P., Šoukal F., Opravil T., Havlica J. & Brandštetr J. (2011) The kinetic analysis of the thermal decomposition of kaolinite by DTG technique. *Powder Technology*, **208**, 20–25.

Reynolds R.C. & Bish D.L. (2002) The effects of grinding on the structure of a low-defect kaolinite. *American Mineralogist*, **87**, 1626–1630

Ríos C.A., Williams C.D. & Fullen M.A. (2009) Nucleation and growth history of zeolite LTA synthesized from kaolinite by two different methods. *Applied Clay Science*, **42**, 446–454.

Sarikaya Y., Önal M., Baran B. & Alemdaroğlu T. (2000) The effect of thermal treatment on some of the physicochemical properties of a bentonite. *Clays and Clay Minerals*, **48**, 557–562.

Scheckel K.G., Luxton T.P., Elbadawy A.M., Impellitter C.A. & Tolaymat T.M. (2010) Synchrotron speciation of silver and zinc oxide nanoparticles aged in a kaolin suspension. *Environmental Science & Technology*, **44**, 1307–1312.

Šesták J. (1984) *Thermal Analysis. Part D, Thermophysical Properties of Solids: their Measurements and Theoretical Thermal Analysis*. Thermophysical Properties of Solids, vol. **12**. Elsevier, New York.

Shvarzman A., Kovler K., Grader G.S. & Shter G.E. (2003) The effect of dehydroxylation/amorphization degree on pozzolanic activity of kaolinite. *Cement and Concrete Research*, **33**, 405–416.

Tang W.J., Liu Y.W., Zhang H. & Wang C.X. (2003) New approximate formula for Arrhenius temperature integral. *Thermochimica Acta*, **408**, 39–43.

Traoré K., Gridi-Bennadji F. & Blanchart P. (2006) Significance of kinetic theories on the recrystallization of kaolinite. *Thermochimica Acta*, **451**, 99–104.

Voll D., Lengauer C., Beran A. & Schneider H. (2001) Infrared band assignment and structural refinement of Al-Si, Al-Ge and Ga-Ge mullites. *European Journal of Mineralogy*, **13**, 591–604.

Voll D., Angerer P., Beran A. & Schneider H. (2002) A new assignment of IR vibrational modes in mullite. *Vibrational Spectroscopy*, **30**, 237–243.

Wang H.Y., Li C.S., Peng Z.J. & Zhang S.J. (2011) Characterization and thermal behavior of kaolin. *Journal of Thermal Analysis and Calorimetry*, **105**, 157–160.

Yang H.M., Du C.F., Hu Y.H., Jin S.M., Yang W.G., Tang A.D. & Avvakumov E.G. (2006) Preparation of porous material from talc by mechanochemical treatment and subsequent leaching. *Applied Clay Science*, **31**, 290–297.

Yao F., Wu Q.L., Lei Y., Guo W.H. & Xu Y.J. (2008) Thermal decomposition kinetics of natural fibers: Activation energy with dynamic thermogravimetric analysis. *Polymer Degradation and Stability*, **93**, 90–98.

Zhuravlev L.T. (1993) Surface characterization of amorphous silica – a review of work from the former USSR. *Colloids and Surfaces A: Physicochemical and Engineering Aspects*, **74**, 71–90.

https://doi.org/10.1180/claymin.2015.050.2.04 Published online by Cambridge University Press